Journal of Nuclear Materials 532 (2020) 152041

Contents lists available at ScienceDirect

Journal of Nuclear Materials

journal homepage: www.elsevier.com/locate/jnucmat

Effects of neutron flux on irradiation-induced hardening and defects in RPV steels studied by positron annihilation spectroscopy

T. Toyama [a, *], T. Yamamoto [b], N. Ebisawa [a], K. Inoue [a], Y. Nagai [a], G.R. Odette [b]

[a] Institute for Materials Research, Tohoku University, Ibaraki, 311-1313, Japan
[b] Materials Department, University of California, Santa Barbara, CA, 93106, USA

ARTICLE INFO

Article history:
Received 26 July 2019
Received in revised form
10 December 2019
Accepted 2 February 2020
Available online 4 February 2020

Keywords:
Reactor pressure vessel steels
Embrittlement
Neutron flux effects
Positron annihilation

ABSTRACT

Neutron-flux effects on irradiation-induced hardening and microstructures in a reactor pressure vessel steel were studied. An A533B-type steel containing no Cu was neutron-irradiated with fluxes of 1×10^{14} n/cm^2/s (high-flux) or 1×10^{12} n/cm^2/s (low-flux) to the same fluence of approximately 3×10^{19} n/cm^2, and the same temperature of approximately 290 °C. The recovery behavior of irradiation-induced defects and irradiation-hardening, ΔHv, was investigated by post-irradiation isochronal annealing from 275 to 450 °C. In both the high- and low-flux cases, the recovery behavior of ΔHv and the average positron lifetime, τ_{ave}, corresponded well to the annealing, suggesting that defects in which positrons are trapped are the origin of irradiation-hardening. The values of $\underline{\Delta Hv}$ and τ_{ave} in the high-flux sample started to recover at around 350 °C, while those in the low-flux sample started to recover at around 400 °C. Thus, in the high-flux sample, unstable defects transiently existing at low temperature but annealed out at around 350 °C, are indicated. Such defects are suggested to be defect-(Mn, Ni, Si) complexes, where the nature of the defect is that of a mono-vacancy and/or dislocation loops.

© 2020 Elsevier B.V. All rights reserved.

1. Introduction

Irradiation-induced embrittlement in reactor pressure vessel (RPV) steels is one of the most important issues for safe operation of nuclear power plants (NPPs) [1,2]. Embrittlement is predicted based on data sets of mechanical tests obtained from surveillance test specimens and specimens irradiated in material testing reactors (MTRs). However, there is frequently a large discrepancy in neutron flux between surveillance test specimens and MTR irradiation, typically about 2–4 orders of magnitude, and the possibility of flux effects has been suggested. For example, it has been reported that the measured ductile-brittle transition temperature (DBTT) for MTR data is higher than the predicted DBTT, whereas the DBTT for surveillance test specimens has been well reproduced [3]. It has been reported that these large differences in flux affect the kinetics of formation of irradiation-induced defects and solute/impurity clusters [4–7], which are widely known as the origin of RPV embrittlement [1,4,8,9], leading to flux effects in the mechanical data sets. For example, so-called "un-stable matrix defects (UMDs)", which exist transiently at low temperatures but anneal out at around 350 °C, may contribute to embrittlement under high-flux conditions [8,10]. In contrast, neither flux effects nor UMDs were reported when European PWR surveillance data were compared with MTR data [11,12]. For long-term safe operation of NPPs, investigation of embrittlement of RPV after a neutron dose several times greater than the expected dose at the end of the NPP lifetime is required. Since MTR data are necessary to obtain such a high dose, the flux effects of surveillance and MTR data on the mechanical properties and microstructures of RPV steels constitute an issue that requires further understanding.

The experimental difficulties of studies on the flux effect arise because the effect depends on a number of parameters other than flux, such as fluence, irradiation temperature, alloy composition of Cu and Ni, the initial state of test samples, and so on [4,8,11–14]. Therefore, a large-scale irradiation program, the irradiation variable program (IVAR), has been performed by the University of California, Santa Barbara (UCSB) group [8], in which systematic neutron irradiation of systematic RPV steels with different fluxes was performed. In this study, we aim to investigate the effects of flux on irradiation-hardening and microstructures for an RPV steel containing no Cu, irradiated with different fluxes, at the same dose and temperature.

* Corresponding author.
E-mail address: t.toyama@tohoku.ac.jp (T. Toyama).

https://doi.org/10.1016/j.jnucmat.2020.152041
0022-3115/© 2020 Elsevier B.V. All rights reserved.

Table 1
Chemical composition of the studied steel in weight percent.

Steel	Cu	Ni	Mn	Mo	P	C	Si	S
LG	0.00	0.74	1.37	0.55	0.005	0.16	0.22	≤0.015

Table 2
Neutron irradiation conditions.

	Flux [n/cm^2/s]	Fluence [n/cm^2]	Temperature [°C]
High-flux	1E+14	3.3E+19	300 ± 5
Low-flux	1E+12	3.4E+19	290 ± 5

As mentioned above, irradiation-induced defects and solute/impurity clusters are the sources of irradiation-hardening (embrittlement), but are difficult to observe directly, even using state-of-the-art high-resolution transmission electron microscopy, because of their very small sizes. In this study, positron annihilation spectroscopy (PAS) and three-dimensional atom probe (3D-AP) are employed to investigate those microstructures. PAS is a unique technique for detecting and characterizing open-volume at the atomic scale size and, thus is appropriate for investigation of irradiation-induced defects. Chemical analysis of positron trapping sites is also available, enabling detection of defect-solute/impurity complexes [15,16]. 3D-AP can map out the alloying elements in three-dimensional space with near-atomic resolution, and reveal elemental distributions and solute/impurity clusters [17,18]. Post-irradiation isochronal annealing (PIA) for the two samples irradiated at high- or low-flux were also performed.

2. Experimental

Several series of A533B-type steels with systematic variations of Cu and Ni content were fabricated by UCSB. The steel investigated in this study, denoted LG, was selected from the LV-series material set. This steel contains no Cu, as listed in Table 1. The heat treatment was as follows: austenitization at 900 °C for 1 h, air cooling, tempering at 600 °C for 40 h, furnace cooling to 300 °C, then air cooling [19,20]. Table 2 shows the neutron irradiation conditions for high- and low-flux irradiation. High-flux irradiation was performed at BR2 in SCK/CEN with a flux of 1×10^{14} n/cm^2/s ($E_n > 1$ MeV) at a temperature of 300 ± 5 °C to a fluence of 3.3×10^{19} n/cm^2, and low-flux irradiation was performed at the University of Michigan Ford Nuclear Reactor under the IVAR program with a flux of 1×10^{12} n/cm^2/s ($E_n > 1$ MeV) at a temperature of 290 ± 5 °C to a fluence of 3.4×10^{19} n/cm^2. Following neutron irradiation, the samples were cut into approximately $5 \times 5 \times 1$ mm^3 sheets using an electro-discharge cutter, and chemically polished with a solution of 5% hydrofluoric acid and 85% hydrogen peroxide. PIA was performed at temperatures from 275 to 450 °C in 25 °C steps. The annealing time for each step was 20 min.

Positron lifetime measurements were carried out using a fast digital oscilloscope and BaF_2 scintillators with a time resolution of approximately 180 ps at full-width at half-maximum. Positron source was ^{22}NaCl of approximately 2 MBq, sealed with Kapton films. A total of 5×10^6 coincidence events were accumulated for each measurement, and the lifetime spectrum was analyzed using the PALSfit software package [21]. The average positron lifetime, τ_{ave}, for the un-irradiated sample was 124 ± 0.2 ps, slightly longer than the positron lifetime in Fe bulk, 106 ps [22], showing slight positron trapping at defects with open volume in the un-irradiated sample.

Coincidence Doppler broadening (CDB) spectra of the positron annihilation radiation were obtained using two Ge detectors in a coincidence arrangement. The coincidence measurements provide less background than when using a single detector set-up by three orders of magnitude, and enable us to measure the momentum distribution of the core electrons specific to each element in the high-momentum region [23]. A total of at least 3×10^6 coincidence events were accumulated for each measurement. The overall momentum resolution was approximately 4×10^{-3} m_0c, where m_0 is the electron rest mass and c is the speed of light.

When positrons are trapped at defects with open volume, they have higher probability of annihilation with conduction electrons spreading out from the surrounding region into the open volumes of the defects than when positrons are delocalized in bulk [24]. The probability of positron annihilation with core electrons is therefore lower. Since conduction electrons have a spatially broad distribution in real space, their distribution in momentum space is narrow and limited to the low-momentum region due to the uncertainty principle. Similarly, the momentum distribution of core electrons is broad and spreads up to the high-momentum region. Therefore, positron trapping at defects with open volume results in an increase in the low-momentum region and a decrease in the high-momentum region of the CDB spectrum. Furthermore, the distribution in high-momentum region reflects the chemical environment of the positron trapping site due to the strong contribution of core electrons to the high-momentum region. This enables chemical analysis at the positron trapping sites. In this study, correlations between the low-momentum component fraction (LCF) and the high-momentum component fraction (HCF) were used to demonstrate the CDB spectra quantitatively. The LCF and the HCF are defined as the ratios of the counts in the low-momentum and high-momentum regions of the CDB spectrum to the total CDB counts, respectively [25]. In this study, the momentum regions were set at $(0-4) \times 10^{-3}$ m_0c and $(15-25) \times 10^{-3}$ m_0c, respectively. Positron trapping at defects with open volume results in an increase in LCF and a simultaneous decrease in HCF. HCF is also sensitive to the chemical environment of the positron trapping site.

For the as-irradiated samples, 3D-AP measurements were performed. Needle samples for 3D-AP measurements were also prepared via a micro-sampling method using a focused ion beam (FIB) [26], where the damaged layer induced by high-energy Ga ions was carefully removed during final milling using a 5 kV Ga ion beam. 3D-AP measurement was carried out using a laser-assisted local-electrode type atom probe by IMAGO Scientific Instruments, LEAP-3000XHR, at an evaporation rate of 0.4 per laser pulse, applying a laser power of 20 nJ, a laser pulse repetition rate of 200 kHz, a DC voltage usually in the range from 3 to 8 kV, and a base specimen temperature of 35 K. All datasets were analyzed using dedicated software, IVAS 3.6.4 by IMAGO Scientific Instruments.

The Vickers micro hardness, Hv, was measured using a Vickers micro hardness tester by SHIMADZU, HMV-2T, with a load of 5 N and a dwell time of 15 s. At least 20 tests were performed for each measurement.

3. Results

Fig. 1 (a) shows the PIA behavior of the hardening, $\Delta Hv = Hv - Hv_{un\text{-}irrad.}$, for the high- and low-flux samples. Hv for the un-irradiated sample was 193 ± 5. In the as-irradiated state, ΔHv was 25 ± 0.3 for the high-flux and 15 ± 0.3 for the low-flux, respectively. It should be noted that the irradiation-hardening for the high-flux was higher than that for the low-flux, although the neutron fluence was almost the same for each. For the high-flux sample, ΔHv started to recover at around 350 °C, and fully recovered at 400 °C. On the other hand, for the low-flux sample, ΔHv was almost constant until 375 °C. The start of recovery was around 400 °C and full recovery

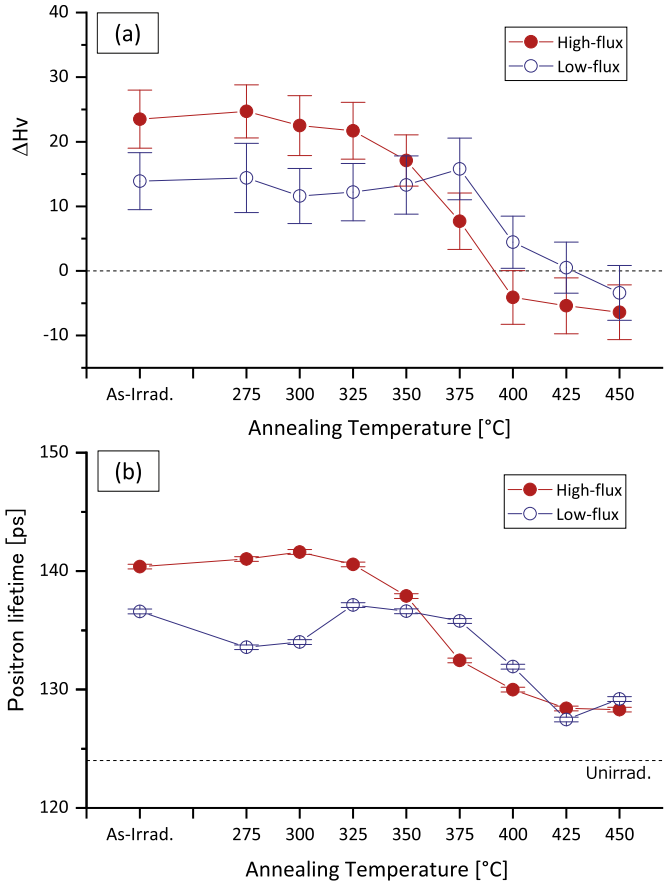

Fig. 1. Post-irradiation isochronal annealing behaviors. (a) Hardening (ΔHv), (b) Average positron lifetime (τ_{ave}).

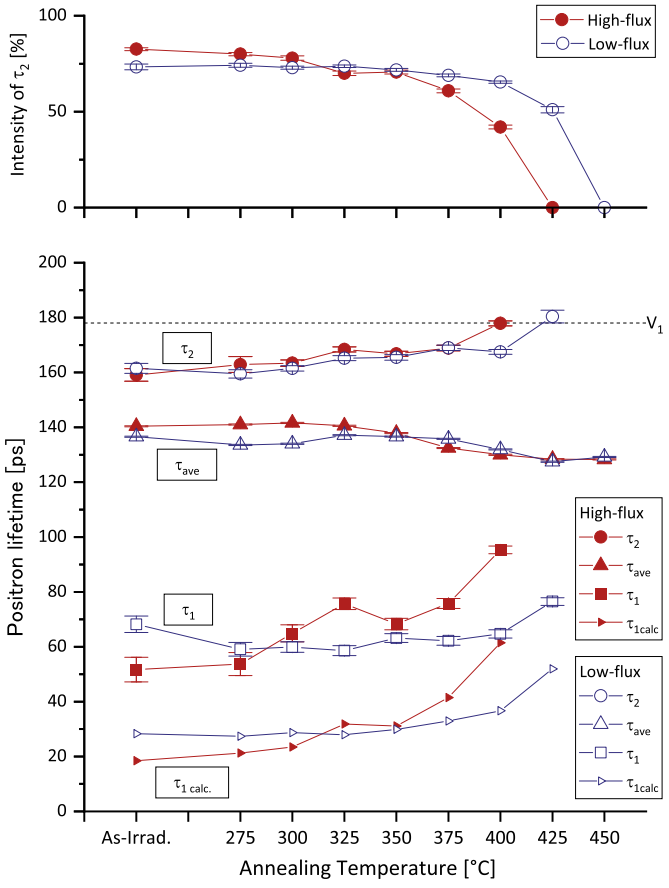

Fig. 2. Post-irradiation isochronal annealing behaviors of positron lifetime.

was at 425–450 °C; these temperatures were higher than in the high-flux case. At 450 °C, *Hv* was slightly lower than that for the un-irradiated sample. This may be some effect on the specimen preparation microstructures at the surface that results in a tiny amount softening at around 450 °C. Whatever else it might be, the observed lower *Hv* will not be significant.

Fig. 1 (b) shows the PIA behavior of τ_{ave} for the high- and low-flux samples. In the as-irradiated state, τ_{ave} was 140 ± 0.3 ps for the high-flux and 137 ± 0.3 ps for the low-flux samples, respectively, longer than that of the un-irradiated state. The increase in τ_{ave} under irradiation can be attributed to positron trapping at irradiation-induced defects. As with the hardening behavior, τ_{ave} for the high-flux samples was higher than for the low-flux samples, although the neutron fluence was almost the same. For the high-flux sample, τ_{ave} started to recover at around 350 °C, while for the low-flux sample, the start of recovery of τ_{ave} was at a higher temperature of around 400 °C. It should be noted that the PIA behavior of ΔHv and τ_{ave} were very similar to each other, suggesting that irradiation-induced defects in which positrons are trapped contribute to irradiation-hardening.

Positron lifetime spectra were decomposed into two components in many cases, as shown in Fig. 2. The calculated positron lifetime at mono-vacancy in pure Fe, 178 ps [22], is also shown by the dashed line. In the high-flux samples, the long lifetime component, τ_2, was approximately 160 ps in the as-irradiated state, suggesting positron trapping was mostly at sites somewhat smaller than mono-vacancy, e.g., dislocation loops, vacancy-solute complexes, vacancy on edge-dislocations [27,28]. The short lifetime component, τ_1, was approximately 50 ps in the as-irradiated state. Such small value, shorter than the value for positron annihilation in Fe bulk (106 ps), is because $\tau_1 = 1/(\lambda_{bulk} + \kappa_{defect})$, where λ_{bulk} is the annihilation rate of positron at bulk and κ_{defect} is the trapping rate of positron to defect, according to two-state trapping model of positron annihilation [29]. With PIA, τ_2 became slightly longer and its relative intensity, I_2, decreased. At 425 °C, τ_2 disappeared and the lifetime spectra were well-fitted with one component. The τ_{ave} after 425 °C annealing was 128 ± 0.3 ps, similar to that in the un-irradiated state. A similar tendency was observed in the low-flux sample; τ_2 disappeared at 450 °C, a slightly higher temperature than in the high-flux samples.

Fig. 3 shows the correlation between the LCF and the HCF in coincidence Doppler broadening of positron annihilation spectroscopy for the high-and low-flux samples. Fig. 3 (a) shows, for reference, the LCF and the HMF of well-annealed pure metals (Fe, Cu, Ni, Mn) and neutron-irradiated pure Fe (irradiated at Japan Materials Testing Reactor at approximately 100 °C to a fluence of 8.3×10^{18} n/cm^2 ($E_n > 1$ MeV), or at 290 ± 3 °C to a fluence of 2.1×10^{19} n/cm^2 ($E_n > 1$ MeV)). Positron lifetime are $\tau_1 = 191 \pm 8$ ps, $\tau_2 = 436 \pm 2$ ps, $I_2 = 82 \pm 1\%$ for the Fe irradiated at 100 °C, and $\tau_1 = 142 \pm 6$ ps, $\tau_2 = 401 \pm 10$ ps, $I_2 = 32 \pm 2\%$ for the Fe irradiated at 290 °C. Positron trapping at vacancy clusters are obvious in neutron-irradiated Fe both at 100 °C and 290 °C because of the large value of τ_2 (>400 ps), however, the Fe neutron-irradiated at 100 °C gives more "pure" component of positron annihilation at vacancy clusters. The reason for this is some of the vacancy clusters are recovered at 290 °C. Therefore, the correlation point for Fe neutron-irradiated at 100 °C is employed as the indicator of positron trapping at vacancy-type defects; The straight line in Fig. 3 (a) and (b) connects the correlation points of well-annealed Fe and Fe

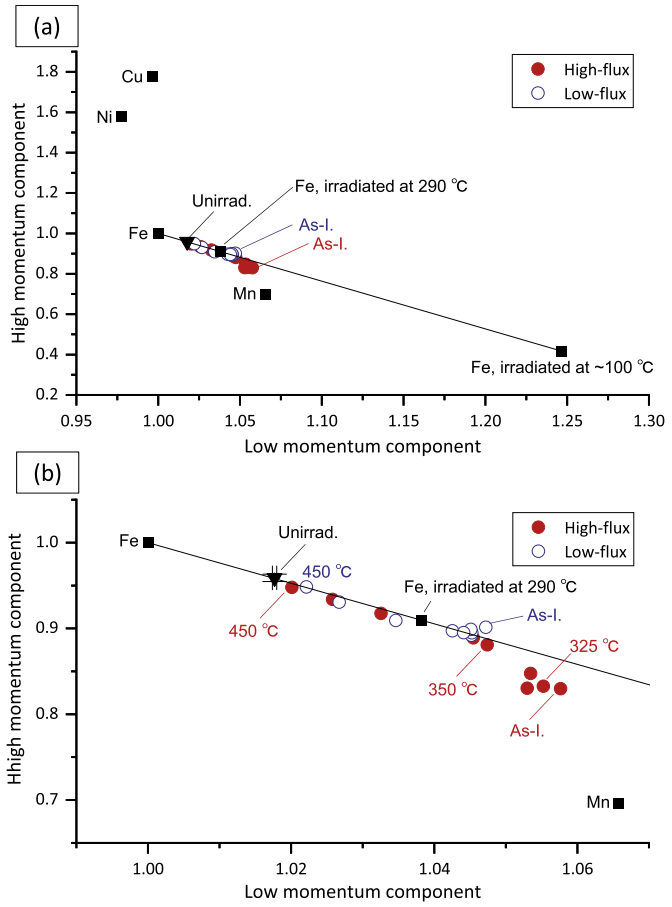

Fig. 3. Post-irradiation isochronal annealing behaviors of the Low- and High-momentum component in coincidence Doppler broadening of positron annihilation radiation. (a) Overview, (b) Enlarged. The error bars for the un-irradiated sample is shown in (b). The error bars for other points are the same extent.

neutron-irradiated at 100 °C. Note that the correlation point for Fe neutron-irradiated at 290 °C is on the line.

Fig. 3 (b) shows an enlarged view of Fig. 3 (a). In the un-irradiated state, the correlation point is located on the straight line, indicating that the positrons are trapped in defects with open volume surrounded entirely Fe. In the high-flux sample, the LMF in the as-irradiated state was higher and the HMF was lower than in the un-irradiated state. This reflects positron trapping at irradiation-induced defects as mentioned in Figs. 1 and 2. It should be noted that the correlation point was located below the straight line, close to the correlation point of Mn. This suggests positron annihilation with electrons of both Fe and Mn. In other words, complexes of defects with open volume and Mn atoms may be formed. The LCF decreased and the HCF increased with increasing PIA temperature. Up to 325 °C, the correlation points were located below the straight line, then on the line at 350 °C, and moving toward the correlation point of the un-irradiated state with further PIA. Both the LCF and the HCF recovered at 450 °C.

In the low-flux sample, the correlation point in the as-irradiated state was located almost on the straight line. Strictly speaking the HCF was higher than that in the straight line, implying positron annihilation with electrons of Ni. This is clearly different from the case in the high-flux sample in the as-irradiated state. The correlation points after 275 °C annealing were located on the straight line, suggesting positron annihilation with electrons of only Fe, and not of Mn. The LMF in the as-irradiated state was lower than in the high-flux sample, which is consistent with the lower τ_{ave} rather than that in the high-flux sample shown in Fig. 1 (b). With the PIA, the correlation point moved on the straight line toward the correlation point of the un-irradiated state, implying that the complexes of defects with open volume and Mn, which are suggested in the high-flux samples, may not be formed in the low-flux samples. The LCF and the HCF recovered at 450 °C, whereas the recovery for the low-flux sample was slightly slower than for the high-flux sample. This is consistent with the recovery behavior of the positron lifetime shown in Fig. 2.

Fig. 4 shows 3D-AP measurements of the un-irradiated sample and the high-, low-flux samples in the as-irradiated state. All the ions in the overlapping $^{58}Fe/^{58}Ni$ peak in the mass spectrum in 3D-AP measurements were assigned to be Fe in order to distinguish dilute Ni clustering. The concentration of Ni, Mn and Si observed by 3D-AP as shown in Fig. 4 are listed in Table 3. In Fig. 4, there was no visual evidence for clustering of Ni, Mn or Si for either sample. Then a cluster analysis algorithm based on the maximum separation method [30] was performed for both samples in order to detect very fine clusters/fluctuations that is difficult for visual observation. The analysis was performed for each distribution of Ni, Mn and Si and the distribution of Ni + Mn + Si with the maximum separation between the solutes (d_{max}) and the minimum number of the solutes (N_{min}). Several values of d_{max} and N_{min} were chosen in the similar method in Ref. [31], and the same volume (20 nm in diameter and 70 nm in length) of each material condition was analyzed. The number of clusters "detected" under each condition are listed in Table 4 (in some cases, "clusters" are detected even in the un-irradiated sample, suggesting overlarge d_{max} and/or too small N_{min}). The 3D-AP results listed in Table 4 indicate no evidence was found for the formation of clusters containing Ni, Mn and Si as a result of irradiation, a result consistent with the visual observations from Fig. 4, despite the potential defect-Mn complexes implied by PAS in the high-flux sample.

4. Discussion

The PIA behavior of ΔHv shown in Fig. 1 (a) showed that the recovery of $\underline{\Delta Hv}$ in the high-flux sample started at around 350 °C, a lower temperature than that in the low-flux sample. This indicates that unstable defects, which are transiently existing at low temperatures but annealed out at around 350 °C, are formed in the high-flux sample. Such defects may contribute the higher ΔHv in the high-flux sample in the as-irradiated state. It should be noted that the irradiation experiments were performed at slightly different temperatures; 300 ± 5 °C for the high-flux and 290 ± 5 °C for the low-flux. Since the higher irradiation temperature (i.e. the high-flux case in this study) generally enhance the recovery of irradiation defects, both hardening and positron lifetime would be smaller than the case of low flux. Nevertheless, the high-flux case showed higher hardening and higher positron lifetime, indicating the exist of UMD.

The PIA behavior of ΔHv and τ_{ave} corresponded well as shown in Fig. 1 (a) and (b). In the high-flux sample, both ΔHv and τ_{ave} in the as-irradiated state were higher than those in the low-flux sample, and both ΔHv and τ_{ave} started to recover at 350 °C. In the low-flux sample, both ΔHv and τ_{ave} were almost constant through the as-irradiated state and 375 °C, and started to recover at 400 °C. Therefore, defects in which positrons are trapped are likely the origin of the irradiation-hardening in the high- and the low-flux samples. Considering the long component of positron lifetime τ_2 shown in Fig. 2., the open volume size of those defects is approximately the mono-vacancy size or somewhat smaller. The candidates for those defects are dislocation loop without solute atoms, vacancy with solute atoms and dislocation loop with solute atoms.

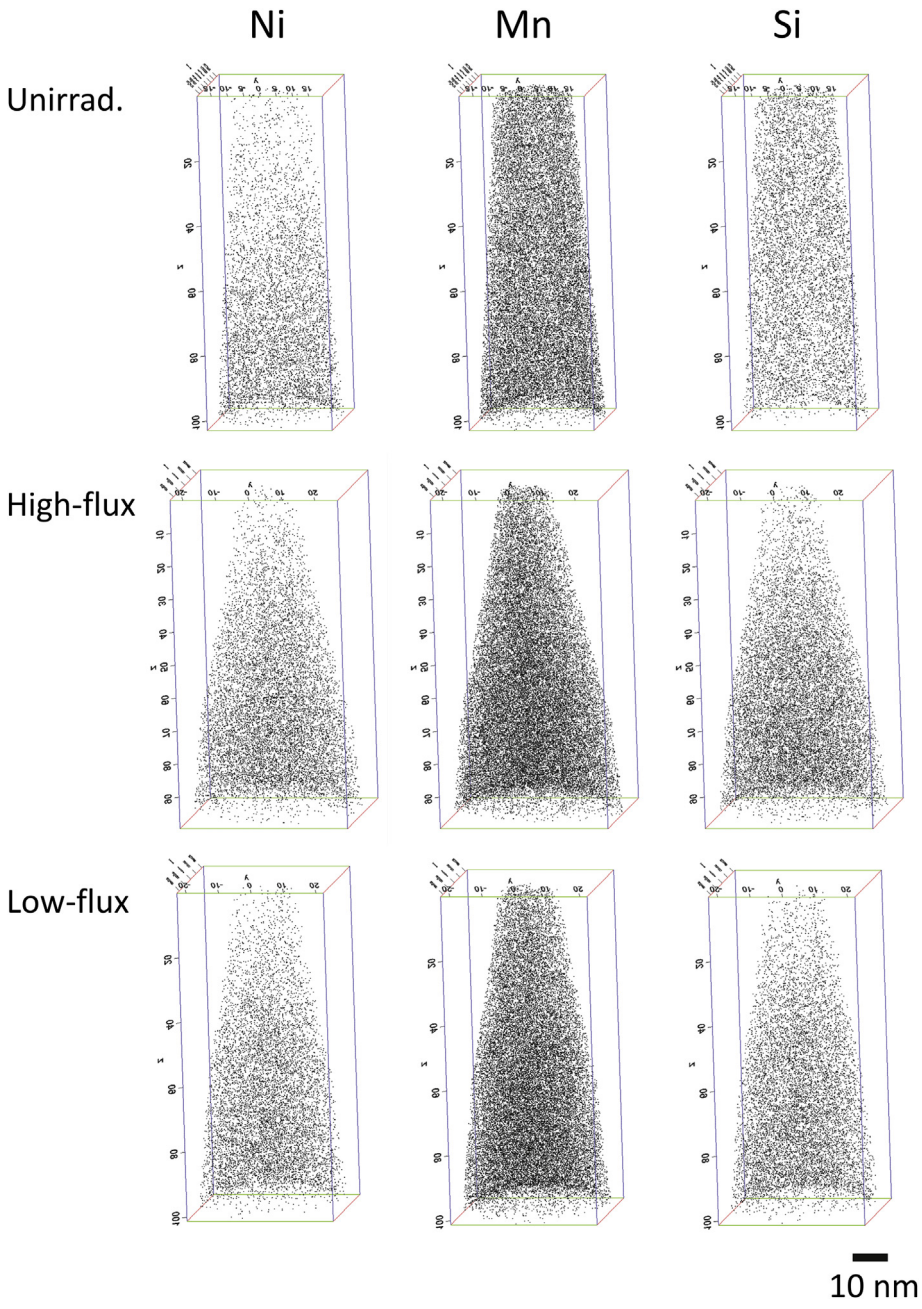

Fig. 4. Elemental maps of three-dimensional atom probe measurements for the un-irradiated and the as-irradiated samples (the high-flux and the low-flux).

Table 3
Concentration of Ni, Mn and Si obtained by three-dimensional atom probe measurements for the un-irradiated and the as-irradiated samples (the high-flux and the low-flux). The nominal concentration of Ni, Mn and Si in the steel is also listed.

	Nominal [wt.%]	Observed [wt.%]		
		Unirrad.	High-flux	Low-flux
Ni	0.74/0.24[a]	0.19	0.22	0.19
Mn	1.37	1.08	1.05	1.17
Si	0.22	0.18	0.17	0.19

[a] Excluding ^{58}Ni.

In the temperature range through the as-irradiated samples to 325 °C, in which higher ΔHv and τ_{ave} were observed in the high-flux sample, positron annihilation with Mn electrons is suggested by CDB measurements, as shown in Fig. 3 (b). Therefore, a defect-Mn complex is strongly suggested in the high-flux sample. On the other hand, no clusters were found with 3D-AP measurements as shown in Fig. 4. Such invisibility of defect-Mn complex may be due to the size of the complex; the trajectory aberrations for evaporated ions in 3D-AP measurements lead to the invisibility of small features such as the defect-Mn complexes [32]. Relatively high concentration of Mn in the matrix also causes the invisibility. From Table 4, it is implied that the (Ni, Mn, Si) clustering could be detected when the number of clustering atoms (i.e., total of Ni + Mn + Si atoms) is more than 10–12 atoms, assuming that no cluster is formed in the un-irradiated sample. In other words, the detection limit of number of clustering atoms is around 10–12. Considering the detection efficiency of 0.37, the detection limit would be approximately 30. Thus, the number of solute atoms

Table 4
Number of solute cluster detected by the cluster analysis in the volume of $\phi 20 \times 70$ nm^3 for the un-irradiated and the as-irradiated samples (the high-flux and the low-flux).

	d_{max}	N_{min}	Number of cluster detected by cluster analysis		
			Unirrad.	High-flux	Low-flux
Ni	0.85	5	10	10	9
	0.85	7	3	3	2
	0.85	9	0	0	0
Mn	0.7	6	60	67	63
	0.7	8	12	13	11
	0.7	10	0	0	0
	0.7	12	0	0	0
Si	0.85	5	11	12	11
	0.85	7	1	0	0
	0.85	9	0	0	0
Ni + Mn + Si	0.6	6	82	90	83
	0.6	8	13	14	14
	0.6	10	3	4	4
	0.6	12	0	0	0

associated with defects is suggested to be less than around 30, i.e. $n < 30$ for the defect-(Ni, Mn, Si)$_n$ complex, where n is the total atom number of Ni, Mn and Si. As mentioned above, the defect is considered to be mono-vacancy and/or dislocation loop.

On the other hand, in the high-flux sample, the Mn concentration in such solute-defect complexes seems to be higher than in the low-flux sample. Burke et al. performed neutron irradiation on A508 steels with 0.05–0.10 wt% Cu in different conditions; at approximately 10^{-7} dpa/s at approximately 239 °C to the dose of 0.017 dpa, and at approximately 10^{-10} dpa/s at approximately 265 °C to the dose of 0.011 dpa, and investigated flux effects on the PIA behavior of hardening and nano-structures [33]. They reported early recovery of irradiation-hardening and non-random distribution of Mn and Ni atoms in the high-flux irradiation (10^{-7} dpa/s), which are fairly similar to the results here. Theoretical studies suggest that Mn has a strong interaction with interstitial atoms [34,35], and Mn trapping at interstitial loops is experimentally implied in neutron- or ion-irradiated model alloys [36,37]. These results support the formation of the defect-Mn complexes suggested in this study.

In the high-flux condition, Mn–Ni–Si clusters with a radius of 0.7 nm and a number density of 5.3×10^{17}/cm^3 were formed after neutron-irradiation to the fluence of 1.3×10^{20} n/cm^2 in LG steel [38], the same steel in the present study. This difference may be attributed to the higher neutron fluence in Ref. [38]; approximately four times higher than in this study.

In general, high-flux irradiation enhances the interaction of irradiation-induced defects with each other [7–9], leading to a decrease in defect mobility via the formation of defect clusters such as interstitial-loops and vacancy clusters. This impedes defect annihilation to sinks and, thus, defects may remain at a high density in the as-irradiated state, as confirmed by the high τ_{ave} and LCF in the high-flux sample observed in this study. Such high defect densities, probably associated with Mn, cause the higher ΔHv in the high-flux sample in the as-irradiated state shown in Fig. 1 (a). The reason that there are more of the defects, which are presumably UMD [8], at the high flux is that they dissolve in temperature dependent annealing time, t_a, thus there are more of them at steady state as $N_{SS} = G/t_a$, where N_{SS} is steady-state number density and G is defect generation rate [39,40].

As a whole, the hardening mechanisms in the low- and high-flux cases are considered below; for the low-flux case, interstitial-clusters (i.e. dislocation loops) and vacancy-type defects are formed in the as-irradiated state, and contribute to the hardening. Since mono-vacancy cannot independently survive at around 300 °C, the vacancy-type defect should be vacancy-solute complexes. For the high-flux case, the interstitial clusters and the vacancy-type defects are formed as well in the as-irradiated state. It should be noted that the number density and/or size of the interstitial clusters in the high-flux sample might be smaller than in the low-flux condition, as mentioned in above paragraph. In addition to the interstitial clusters and the vacancy-type defects, UMD is also formed in the high-flux. The nature of UMD is suggested to be a defect in which more Mn is associated. During PIA, the UMD annealed out up to 350 °C but the interstitial clusters still exists after 350 °C. The observed high ΔHv after 350 °C in the low-flux sample might be attributed to the interstitial clusters.

5. Conclusion

An A533B steel with no Cu were neutron-irradiated with a flux of 1×10^{14} n/cm^2/s or 1×10^{12} n/cm^2/s at the same fluence and temperature. The recovery behavior of ΔHv and irradiation-induced defects were investigated by PIA from 275 to 450 °C in 25 °C steps. In both the high- and low-flux conditions, the recovery behavior of ΔHv and average positron lifetime, τ_{ave}, corresponded well with the PIA, indicating that defects in which positrons are trapped are the origin of irradiation-hardening. In the high-flux sample, the recovery of ΔHv and τ_{ave} started at around 350 °C, 50 °C lower than in the low-flux sample. Thus, unstable defects transiently existing at low temperature but annealed out at around 350 °C are present in the high-flux sample. Such defects are suggested to be defect-(Mn, Ni, Si) complexes, where the nature of the defect is that of a mono-vacancy and/or dislocation loops.

Declaration of competing interest

TT, NE, KI and YN were supported by Grant-in-Aids for Scientific Research of MEXT (Nos. 26709073 and 17H03517).

TY and GRO were funded by DOE NEUP grant, DE-AC07-05ID14517.

CRediT authorship contribution statement

T. Toyama: Investigation, Writing - original draft. **T. Yamamoto:** Resources, Writing - review & editing. **N. Ebisawa:** Visualization. **K. Inoue:** Validation. **Y. Nagai:** Supervision, Project administration, Funding acquisition. **G.R. Odette:** Conceptualization, Resources, Writing - review & editing.

Acknowledgements

This work was partially supported by Grant-in-Aids for Scientific Research of MEXT (Nos. 26709073 and 17H03517). The authors thank M. Yamazaki and K. Suzuki for their support with hot laboratory work. Work at UCSB was funded by DOE NEUP grant, DE-AC07-05ID14517.

References

[1] G.E. Lucas, An evolution of understanding of reactor pressure vessel steel embrittlement, J. Nucl. Mater. 407 (1) (2010) 59–69.
[2] G.R. Odette, T. Yamamoto, T.J. Williams, R.K. Nanstad, C.A. English, On the histroy and status of reactor pressure vessel steel ductile to brittle transition temperature shift predictioni models, J. Nucl. Mater. 526 (2019) 151863.
[3] G.R. Odette, R.K. Nanstad, Predictive reactor pressure vessel steel irradiation embrittlement models: issues and opportunities, JOM (J. Occup. Med.) 61 (7) (2009) 17–23.
[4] G.R. Odette, B.D. Wirth, A computational microscopy study of nanostructural evolution in irradiated pressure vessel steels, J. Nucl. Mater. 251 (1997) 157–171.

[5] B.D. Wirth, A. Caro, G.R. Odette, Dynamics of self-interstitial cluster migration in pure a-Fe and Fe-Cu alloys, Phys. Rev. B 65 (2002) 144102.
[6] J. Marian, B.D. Wirth, R. Schaublin, G.R. Odette, J. Manuel Perlado, MD modeling of defects in Fe and their interactions, J. Nucl. Mater. 323 (2003) 181–191.
[7] R.E. Stoller, The Effect of Neutron Flux on Radiation-Induced Embrittlement in Reactor Pressure Vessel Steels, ASTM, 2004, pp. 1–12.
[8] G.R. Odette, T. Yamamoto, D. Klingensmith, On the effect of dose rate on irradiation hardening of RPV steels, Phil. Mag. 85 (4–7) (2005) 779–797.
[9] K. Fukuya, Current understanding of radiation-induced degradation in light water reactor structural materials, J. Nucl. Sci. Technol. 50 (3) (2013) 213–254.
[10] G.R. Odette, G.E. Lucas, Embrittlement of nuclear reactor pressure vessels, J. Occup. Med. 53 (7) (2001) 18–22.
[11] R. Chaouadi, R. Gerard, Neutron flux and annealing effects on irradiation hardening of RPV materials, J. Nucl. Mater. 418 (1–3) (2011) 137–142.
[12] R. Chaouadi, R. Gerard, Confirmatory investigations on the flux effect and associated unstable matrix damage in RPV materials exposed to high neutron fluence, J. Nucl. Mater. 437 (1–3) (2013) 267–274.
[13] L. Debarberis, F. Sevini, B. Acosta, A. Kryukov, D. Erak, Fluence rate effects on irradiation embrittlement of model alloys, Int. J. Pres. Ves. Pip. 82 (5) (2005) 373–378.
[14] F. Bergner, A. Ulbricht, H. Hein, M. Kammel, Flux dependence of cluster formation in neutron-irradiated weld material, J. Phys. Condens. Matter 20 (10) (2008) 104262.
[15] T. Toyama, Y. Nagai, Z. Tang, M. Hasegawa, A. Almazouzi, E. van Walle, R. Gerard, Nanostructural evolution in surveillance test specimens of a commercial nuclear reactor pressure vessel studied by three-dimensional atom probe and positron annihilation, Acta Mater. 55 (20) (2007) 6852–6860.
[16] M. Shimodaira, T. Toyama, K. Yoshida, K. Inoue, N. Ebisawa, K. Tomura, T. Yoshiie, M.J. Konstantinovic, R. Gerard, Y. Nagai, Contribution of irradiation-induced defects to hardening of a low-copper reactor pressure vessel steel, Acta Mater. 155 (2018) 402–409.
[17] C. English, J. Hyde, Recent Progress in the Understanding of RPV Embrittlement, 2007.
[18] J.M. Hyde, A. Cerezo, T.J. Williams, Statistical analysis of atom probe data: detecting the early stages of solute clustering and/or co-segregation, Ultramicroscopy 109 (2009) 502–509.
[19] S. Kobayashi, T. Yamamoto, D. Klingensmith, G.R. Odette, H. Kikuchi, Y. Kamada, Magnetic evaluation of irradiation hardening in A533B reactor pressure vessel steels: magnetic hysteresis measurements and the model analysis, J. Nucl. Mater. 422 (1–3) (2012) 158–162.
[20] S. Kobayashi, T. Yamamoto, D. Klingensmith, G.R. Odette, H. Kikuchi, Y. Kamada, Effect of neutron flux on magnetic hysteresis in neutron-irradiated pressure vessel steels, IEEE Trans. Magn. 50 (4) (2014).
[21] J.V. Olsen, P. Kirkegaard, .N.J. P, M. Eldrup, PALSfit: a new program for the evaluation of positron lifetime spectra, Phys. Stat. Sol. C 4 (2007) 4004–4006.
[22] H. Ohkubo, Z. Tang, Y. Nagai, M. Hasegawa, T. Tawara, M. Kiritani, Positron annihilation study of vacancy-type defects in high-speed deformed Ni, Cu and Fe, Mater. Sci. Eng., A 350 (2003) 95.
[23] P. Asoka-Kumar, M. Alatalo, V.J. Ghosh, A.C. Kruseman, B. Nielsen, K.G. Lynn, Increased elemental specificity of positron annihilation spectra, Phys. Rev. Lett. 77 (1996) 2097–2100.
[24] Y. Nagai, Z. Tang, M. Hasegawa, T. Kanai, M. Saneyasu, Irradiation-induced Cu aggregations in Fe: an origin of embrittlement of reactor pressure vessel steels, Phys. Rev. B 63 (2001) 134110.
[25] Y. Nagai, K. Takadate, Z. Tang, H. Ohkubo, H. Sunaga, H. Takizawa, M. Hasegawa, Positron annihilation study of vacancy-solute complex evolution in Fe-based alloys, Phys. Rev. B 67 (2003) 224202.
[26] M.K. Miller, K.F. Russell, Atom probe specimen preparation with a dual beam SEM/FIB miller, Ultramicroscopy 107 (2007) 761–766.
[27] Y. Kamimura, T. Tsutsumi, E. Kuramoto, Calculations OF positron lifetimes IN a JOG and vacancies ON an edge-dislocation line IN FE, Phys. Rev. B 52 (2) (1995) 879–885.
[28] Y. Kamimura, T. Tsutsumi, E. Kuramoto, Influence of dislocations on positron lifetime in iron, J. Phys. Soc. Jpn. 66 (1997) 3090–3096.
[29] R. Krause-Rehberg, H.S. Leipner, Positron Annihilation in Semi-conductors, Springer, 1998.
[30] J.M. Hyde, E.A. Marquis, K.B. Wilford, T.J. Williams, A sensitivity analysis of the maximum separation method for the characterisation of solute clusters, Ultramicroscopy 111 (6) (2011) 440–447.
[31] Y. Dong, A. Etienne, A. Frolov, S. Fedotova, K. Fujii, K. Fukuya, C. Hatzoglou, E. Kuleshova, K. Lindgren, A. London, A. Lopez, S. Lozano-Perez, Y. Miyahara, Y. Nagai, K. Nishida, B. Radiguet, D.K. Schreiber, N. Soneda, M. Thuvander, T. Toyama, J. Wang, F. Sefta, P. Chou, E.A. Marquis, Atom probe tomography interlaboratory study on clustering analysis in experimental data using the maximum separation distance approach, Microsc. Microanal. 25 (2) (2019) 356–366.
[32] J.M. Hyde, G. Sha, E.A. Marquis, A. Morley, K.B. Wilford, T.J. Williams, A comparison of the structure of solute clusters formed during thermal ageing and irradiation, Ultramicroscopy 111 (6) (2011) 664–671.
[33] M.G. Burke, R.J. Stofanak, J.M. Hyde, C.A. English, W.L. Server, Microstructural aspects of irradiation damae in A508 Gr 4N forging steel: composition & flux effects, ASTM 1 (5) (2002) 194–207.
[34] P. Olsson, T.P.C. Klaver, C. Domain, Ab initio study of solute transition-metal interactions with point defects in bcc Fe, Phys. Rev. B 81 (5) (2010), 054102.
[35] L. Messina, M. Nastar, T. Garnier, C. Domain, P. Olsson, Exact ab initio transport coefficients in bcc Fe-X (X=Cr, Cu, Mn, Ni, P, Si) dilute alloys, Phys. Rev. B 90 (10) (2014).
[36] K. Yabuuchi, R. Kasada, A. Kimura, Effect of Mn addition on one-dimensional migration of dislocation loops in body-centered cubic Fe, Acta Mater. 61 (17) (2013) 6517–6523.
[37] H. Watanabe, S. Masaki, S. Masubuchi, N. Yoshida, K. Dohi, Effects of Mn addition on dislocation loop formation in A533B and model alloys, J. Nucl. Mater. 439 (2013) 268–275.
[38] P.B. Wells, T. Yamamoto, B. Miller, T. Milot, J. Cole, Y. Wu, G.R. Odette, Evolution of manganese-nickel-silicon-dominated phases in highly irradiated reactor pressure vessel steels, Acta Mater. 80 (2014) 205–219.
[39] G.R. Odette, E.V. Mader, G.E. Lucas, W.J. Phythian, C.A. English, The effect of flux on irradiation hardening of pressure vessel steels, in: A.S. Kumar (Ed.), 17th International Symposium on Effects of Radiation on Materials, American Society for Testing and Materials, West Conshohocken, 1993, p. 373.
[40] E.V. Mader, Kinetics of Irradiation Embrittlement and the Post-Irradiation Annealing of Nuclear Reactor Pressure Vessel Steels, UC Santa Barbara, UC Santa Barbara, 1995.